Conformational Behavior of Guest Chains in Uniaxially Stretched Poly(diethylsiloxane) Elastomers: ^{2}H NMR and SANS

Ashish Batra,[†] Ronald C. Hedden,[‡] Paula Schofield,[§] Aaron Barnes,[§] Claude Cohen,*,[†] and T. M. Duncan[†]

School of Chemical and Biomolecular Engineering, Olin Hall, Cornell University, Ithaca, New York 14853, Evergreen State College, Olympia, Washington 98505, and Polymers Division, National Institute of Standards and Technology, Gaithersburg, Maryland 20899

Received August 6, 2003; Revised Manuscript Received October 3, 2003

ABSTRACT: [2]H nuclear magnetic resonance (NMR) and small angle neutron scattering (SANS) data are reported for deuterated guest chains of polydiethysiloxane (PDES) in end-linked PDES networks as a function of the molecular weight of guest chains relative to that of the network elastic chains. We exploit the ability of PDES networks to form a strain-induced mesophase to demonstrate the tendency of longer guest chains to phase separate or partition selectively to the amorphous phase and the tendency of smaller guest chains to remain distributed between the mesophase and the amorphous phase. The segmental orientation of the guest chains measured via ^{2}H NMR peak splitting can be interpreted in terms of an enthalpic orientational coupling of the chain segments in the amorphous state. SANS results show that the radius of gyration of guest chains in the unstretched networks and in the networks stretched below the mesomorphic transition remains essentially unchanged from that in the melt state. The scattering intensity from SANS patterns for networks with guest chains of any size has a peak in the direction parallel to the stretch direction that reflects the domain spacing of the lamellae in the mesophase.

1. Introduction

Energetic interactions between chains segments of an elastomer cause deviations from classical theories of rubber elasticity. In mesomorphic and liquid crystalline elastomers, such interactions are thought to be responsible for unique properties such as spontaneous phase changes, discontinuous stress−strain relations, and deviations from the stress-optical rule.[1] PDES elastomers are a class of flexible-chain homopolymer networks similar to liquid crystalline elastomers in that they show such energetic interactions despite the absence of rigid mesogenic groups.[2−4] Endlinked PDES networks prepared from short PDES precursor chains (in the amorphous state) are transparent, amorphous elastomers similar in appearance to silicone rubber (poly(dimethylsiloxane), PDMS). However, upon stretching past a critical extension ratio, the initially amorphous PDES elastomers undergo a strain-induced phase transition to a mesomorphic, conformationally disordered (condis crystal)[5] phase.[6] This spontaneous amorphous-to-mesomorphic transition is accompanied by a macroscopic shape change ("necking" phenomenon) resulting from the molecular-level alignment of neighboring elastic chains in the direction of applied tension. Previously, ^{2}H NMR studies showed that the mesomorphic state in PDES elastomers is a biphasic state consisting of both amorphous and mesophase microdomains.[6,7] Earlier ^{2}H NMR studies of "optimal" PDES networks (defined as containing a minimal amount of topological defects) have shown that an enthalpic orientational coupling exists between elastic PDES segments[6,7] that offsets the entropic penalty for alignment of elastic network chains, stabilizing the mesomorphic state.

[†] Cornell University.
[‡] National Institute of Standards and Technology.
[§] Evergreen State College.

Here we use ^{2}H NMR to examine the conformation of unattached PDES guest chains dissolved in both unstretched and stretched PDES networks. We investigate how the size of the guest chain relative to the mesh size of the network affects the conformation of the guest chain in the amorphous state. In the mesomorphic state, we study how the size of the guest chains affects partitioning between the amorphous and mesophase microdomains.

^{2}H NMR is sensitive to elastomer segment anisotropy through the orientation-dependent quadrupolar interaction that causes a frequency shift related to the time-averaged orientation of C−[2]H bonds. The spectral splitting induced by uniaxial strain may be predicted by averaging the frequency shift over all bond orientations compatible with end-to-end vectors that are preferentially oriented relative to the strain axis.[8] For an elastomer strained along an axis perpendicular to the external magnetic field the splitting is given by

$$\Delta \nu = \frac{3 e^2 qQ}{4h} \langle P_2(\cos \phi) \rangle \langle P_2(\cos \psi) \rangle \tag{1}$$

where ϕ is the angle between a C−[2]H bond and the vector of the segment to which it is attached, e^2qQ/h is the static quadrupolar coupling, and ψ is the angle between the segment vector and the strain axis. Here, $\langle P_2(\cos \psi) \rangle$ is the average of the second Legendre polynomial of cos ψ and represents the segment order parameter *S*. Thus, the NMR splitting is directly proportional to the segment order parameter. Previous work[9] with optimal PDMS networks demonstrated that the spectral splitting and hence the segment orientation was independent of whether a chain was elastic, guest (unattached), or pendent and that the theory of Brereton and Ries[10] based on excluded volume interactions could explain the segment orientation observed with NMR.

Several studies[11−13] have used small angle neutron scattering (SANS) to examine the radius of gyration (R_g)

Table 1. Molar Mass (M_n) and Polydispersity Index (PDI) of the Deuterated Guest Chains[a]

guest chains	M_n (kg mol^{-1})	PDI
d_5–I	71	1.35
d_5–II	45	1.56
d_5–III	40	1.26
d_2–II	43	1.18
d_2–IV	20	1.21
d_2–VII	10	1.19

[a] Uncertainties quoted in text.

of linear probe chains trapped in a polymer network. The results have varied from R_g of guest chains in the network being equivalent to the R_g of the same chains in the melt,[11] to a scaling given by $R_g \propto N_c$, where N_c is the mesh size and N_c is smaller than the degree of polymerization of the linear chain, N_1.[12] Recently, it has been shown that the radius of gyration of linear PDMS chains does not vary as a function of PDMS network mesh size.[13] This result also agrees with recent Monte Carlo simulations.[14]

Here, we use SANS in two series of experiments, first to examine the radius of gyration of PDES probe chains in stretched and unstretched PDES networks in the purely amorphous state. Second, PDES networks containing deuterated free PDES guest chains are stretched and SANS is used to probe the network microstructure of the mesomorphic state. The biphasic mesomorphic state consists of both amorphous and mesophase microdomains.

2. Experimental Procedures

2.1. Samples. Telechelic vinyl-functionalized PDES precursor chains were synthesized from hexaethylcyclotrisiloxane monomer (Gelest, Inc.) by cationic polymerization with trifluoromethanesulfonic acid (Aldrich) as an initiator. Networks were formed by end-linking with the tetrafunctional cross-linker tetrakis(dimethylsiloxy)silane in the presence of a platinum catalyst. Some of the deuterated precursors for ^{2}H NMR studies were synthesized in a similar manner but by mixing in a 1:3 proportion (by mole fraction) of deuterated monomers with $-CD_2CH_3$ ethyl groups to monomers with the $-CH_2CH_3$ groups. Using $-CD_2CH_3$ rather than $-CD_2CD_3$ monomer was convenient for NMR studies because $-CD_2$ deuterons are more closely coupled to the Si–O backbone segments whereas the signal in $-CD_2CD_3$ is complicated by the methyl group. Three fractions labeled d_2-II, -IV and -VII obtained by fractionation with a toluene/methanol system were used in the study and are described in Table 1. The details of the synthesis and cross-linking procedure have been reported in an earlier publication.[15]

For SANS studies, two batches of PDES were synthesized: a nondeuterated sample of relatively low molar mass, "PDES-H," and a partially deuterated sample of substantially higher molar mass, "PDES-d_5." Hexa(ethyl-d_5)cyclotrisiloxane was prepared by a method previously described using C_2D_5OH as starting material.[7] In the PDES-d_5 synthesis, 0.33 mole fraction of the deuterated monomer and 0.67 mole fraction of the hydrogen-containing material were mixed prior to polymerization. PDES was prepared by polymerization of hexaethylcyclotrisiloxane monomers using NaOH as catalyst and 12-crown-4 as promoter.[16] PDES samples were washed with water and repeatedly washed in refluxing ethanol to remove catalyst and cyclic byproducts prior to use. From ^{1}H NMR measurements, the

composition of the resulting PDES-d_5 was determined to be 0.317 ± 0.003 mole fraction $-CD_2CD_3$ groups and 0.683 ± 0.003 mole fraction $-CH_2CH_3$ groups. The PDES-d_5 sample was fractionated to yield samples of different molar masses, labeled d_5-I, -II and -III. Weight-average molar masses of 96, 70, and 50 kg mol^{-1} for fractions I–III, respectively, were determined by gel permeation chromatography (GPC) in toluene. The chain characteristics are described in Table 1. Unless otherwise stated, standard uncertainties in GPC molecular masses are estimated as $\pm 10\%$ of the values reported on the basis of one standard deviation.

Blends of the PDES-d_5 fractions at 0.01–0.04 mass fraction in PDES-H were prepared for SANS investigations. In the networks in which PDES-d_5 fractions were present as the guest chains, the networks were cured from a homogeneous mixture containing the guest chains. In networks to which the PDES-d_2 fractions were to be added, a thin layer of these fractions was spread on the surface of the network and allowed to diffuse and homogenize into these networks over a period of 2 months. Care was taken to use a concentration of guest chains lower than that dictated by the equilibrium Flory–Rehner relation[17] and the overlap c^* concentration.[18] For SANS experiments rectangular sheets of $2.5 \times 13 \times 1.25$ mm were made. For ^{2}H NMR experiments, rectangular samples measuring $20 \times 3.5 \times 1.25$ mm were used.

The molar mass of the precursor chains and their polydispersity, the shear modulus of the networks, and the concentrations of guest chains in the networks are reported in Table 2. The samples are arranged in increasing order of the ratio of the molar mass of the guest chains to the molar mass of the network precursor chains. The shear modulus G_e/RT was estimated from a correlation previously established between the shear modulus and equilibrium swelling of the networks in toluene.[15]

2.2. ^{2}H NMR Instrumentation. Spectra were obtained on a Tecmag Apollo HF spectrometer operating at a frequency of 30.723 MHz for deuterium. A Bruker z32vHP probe body with a custom-built probe head and coil was used. The coil designed to minimize dead volume had a length of 8.5 mm, diameter of 7.5 mm, and 19 turns. It was made of 22 gauge copper wire coated with epoxy resin to reduce arcing during the radio frequency (RF) pulses. The elastomers were oriented such that the extension axis was parallel to the coil axis and perpendicular to the applied magnetic field. The stretching device used to stretch the samples in situ has been described in detail elsewhere.[6] To measure local extension ratios, ink dots were marked on the sample and digital images were taken at each overall extension ratio.

The pulse program used was a simple $(90°)_x$ pulse of typical duration 2.5 μs. The repetition delay between scans was 1 s. To achieve a reasonable signal-to-noise ratio, around 7200 scans were required for larger concentrations of probe chains and small extension ratios. As many as 150 000 transients were required for smaller concentrations and large extension ratios. To improve the apparent signal-to-noise ratio, a line broadening of 50 Hz was added to each spectrum. Baseline correction and phase adjustments were carried out on NTNMR (Tecmag) software. ^{2}H NMR spectra were fitted using solver techniques in Microsoft Excel.

2.3. SANS Measurements. SANS measurements were conducted at the National Institute of Standards

Table 2. PDES Network Characteristics (Uncertainties Quoted in Text)

sample	probe chain	precursor			guest		$M_{n,g}/M_{n,h}$
		$M_{n,h}$ (kg/mol)	PDI	G_e/RT (mol/m³)	$M_{n,g}$ (kg/mol)	mass fraction	
1		13	1.14	97.2		0.0	
2	d_2–VII	26	1.27	59.6	10	0.09	0.4
3	d_2–VII	21	1.25	66.4	10		0.5
4	d_2–IV	26	1.27	59.6	20	0.06	0.8
5	d_5–III	27	1.33	56.2	40	0.02	1.5
6	d_2–II	26	1.27	59.6	43	0.025	1.7
7	d_5–III	18	1.18		40	0.025	2.2
8	d_5–I	30	1.20	75.2	71	0.01	2.4
9	d_5–II	18	1.18	84.0	45	0.025	2.5
10	d_5–I	23	1.30	58.0	71	0.01	3.1
11	d_5–I	23	1.30	62.4	71	0.005	3.1

and Technology Center for Neutron Research (NCNR) on the NG3 30 m beamline facility.[19,20] The scattering vector q is defined as

$$q = \frac{4\pi}{\lambda} \sin\left(\frac{\theta}{2}\right) \quad (2)$$

where λ is the incident neutron wavelength and θ is the scattering angle. "High-q" data were recorded with sample to detector distance = 1.35 m (0.03 Å^{-1} < q < 0.45 Å^{-1}), and "low-q" data were recorded with sample to detector distance = 13 m (0.008 Å^{-1} < q < 0.048 Å^{-1}). The neutron wavelength was λ = 6 Å with a spread of $\Delta\lambda/\lambda$ = 0.12. Selected experiments on networks in the mesomorphic state were subsequently conducted on the NG1 8 m facility. The sample to detector distance was 3.84 m, and the neutron wavelength was λ = 6 Å with a spread of $\Delta\lambda/\lambda$ = 0.12.

Data were processed with the software provided by the Center for Neutron Research at NIST. The number of counts was corrected for detector sensitivity and background scattering. Absolute scattering intensities were calculated using the empty beam as a reference. The scattered intensity was corrected for sample transmission using experimental values. The resulting data sets were circularly averaged over the detector angle ϕ to yield absolute scattering intensity I as a function of the scattering vector, q. For cases where scattering was dependent upon detector angle, the scattered intensity at a given angle ϕ was computed by sector or rectangular averaging over a differential angle $\Delta\phi$ or pixel width. Values of $\Delta\phi$ for individual runs are quoted in the text. The uncertainties in the scattering data are calculated as the estimated standard deviation of the mean. The total combined uncertainty is calculated using standard error propagation methods. In cases where the limits are smaller than the plotted symbols, the limits are left out for clarity. Fits of the scattering data were made by a least-squares fit, giving an average and a standard deviation to the fit. The relative uncertainties reported are one standard deviation, based on the goodness of the fit.

The deuterated linear chains were characterized by performing SANS experiments on blends of the deuterated chains with low molecular weight protonated PDES that disrupts the mesophase of the chains. For each deuterated sample, at least three different concentrations between 0.01 and 0.04 mass fraction of the sample in PDES-H were used. An aluminum extension device was constructed to fit snugly into the sample holders of the NG3 SANS instrument and was used to stretch the samples for small extension experiments as well as to stretch the samples into the mesophase. Unless otherwise stated, standard uncertainties in local extension
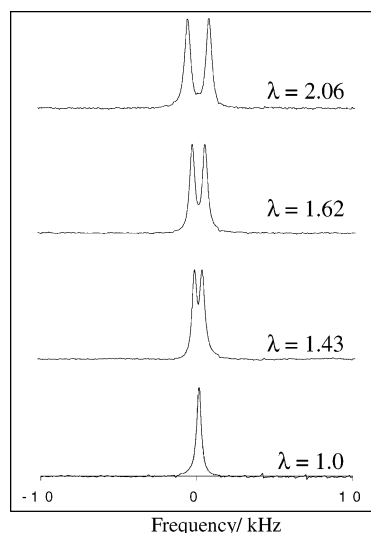

Figure 1. Extension spectra of sample 2 in the amorphous state at different extension ratios.

ratios are assumed to be ±10% based on one standard deviation.

3. Results and Discussion

3.1. ^{2}H NMR Spectra. In the amorphous state, the ^{2}H NMR spectra of stretched protonated PDES networks with –CD$_2$CH$_3$ deuterated guest chains were similar to those of PDES networks with –CD$_2$CH$_3$ deuterated elastic chains. Line widths are narrower because of the increased orientational motional averaging of C–^{2}H bonds in the unattached guest chains. Figure 1 shows spectra for network 2 as a function of extension ratio. These spectra are representative of the amorphous state of all the samples (2–4 and 6) with –CD$_2$CH$_3$ probe chains. The spectra of guest chains in unstretched networks show a single sharp peak of approximately 400 Hz width at half-height that is narrower than that previously observed for elastic chains within an unstretched PDES elastomer, 1 kHz. As the extension ratio is increased, the spectrum splits into two peaks and the splitting increases with increasing local extension ratios. The line shapes could be fitted very well to the sum of two identical Lorentzians. The splitting was taken as the distance between the centers of component peaks. The quadrupolar peak splitting is proportional to the segment order parameter.

Ideal rubber elasticity theories[21,22] as well as predictions from NMR models based only on excluded volume interactions predict that the order parameter and the NMR splitting is proportional to ($\lambda^2 - \lambda^{-1}$). A plot of the splitting as a function of ($\lambda^2 - \lambda^{-1}$) is shown in Figure 2. For conventional elastomers, such a plot is
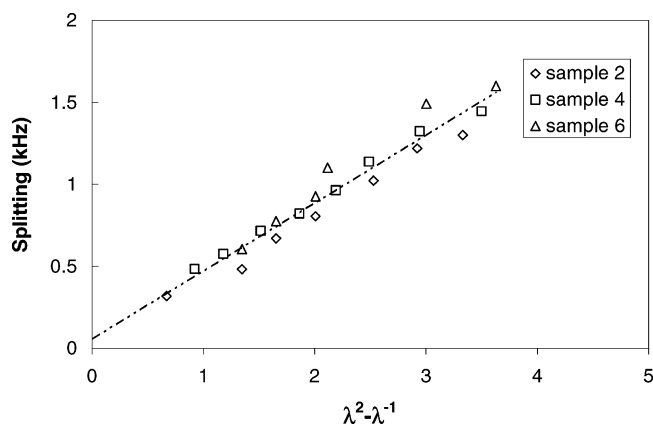
Figure 2. Peak splitting as a function of $\lambda^2 - \lambda^{-1}$ for sample 2, 4, and 6 in the amorphous state.
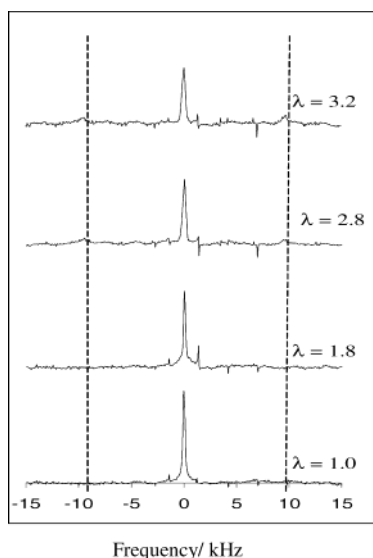

Figure 3. Extension spectra of sample 5. Stretch ratios of 2.8 and 3.2 correspond to the sample being in the mesomorphic state. Lines are guide to the eye for the mesophase splitting of 19.1 kHz.

Figure 4. Extension spectra of sample 2 in the fully necked mesomorphic state.

linear and passes through the origin.[23-25] A nonzero intercept has been observed previously under compression[7] and under extension[6] for optimal deuterated PDES networks with moduli higher than the present samples. This effect has been explained in terms of energetic couplings between chain segments where the chain segments may align locally with each other even in the undeformed state, when the overall orientation is isotropic. For the present samples as in the earlier samples[6] with comparable moduli, the nonzero intercept is not evident. The value of the ratio of peak splitting to $(\lambda^2 - \lambda^{-1})$ for the present samples with guest chains is comparable to its value in networks with deuterated elastic chains of similar modulus as has been observed previously in PDMS elastomers.[9]

The spectra of networks with $-CD_2CD_3$ probe chains (samples 5, 7-11) are dominated by the methyl group and no splitting is observed on stretching in the amorphous state. Figure 3 shows the spectra of sample 5 as a function of local extension ratio. The full width at half-maximum increases from 300 Hz for an unstretched state to 400 Hz for a stretch ratio of 1.8 indicating an increase in order in the system.

3.2. Mesomorphic State. As the local extension ratio is increased beyond 2.2, a neck forms that propagates
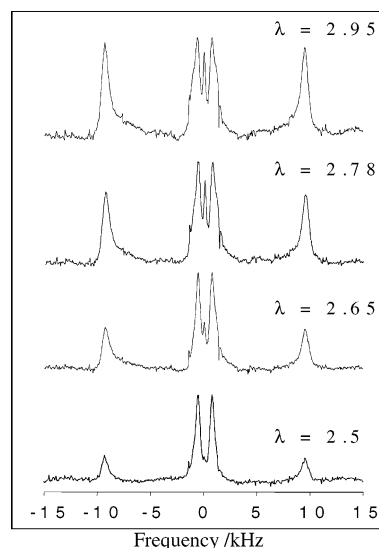
as the local extension ratio is increased. It is here that the effect of relative size of guest chains to the elastic chains is seen. When a mesomorphic neck has been formed, two characteristic mesophase peaks with a splitting of 19.1 kHz appear for samples 2-4 that have guest $-CD_2CH_3$ chains and sample 5 that has guest $-CD_2CD_3$ chains that are smaller than 1.6 times the molar mass of elastic chains. For networks 6-11 that have guest chains that are larger than at least 1.6 times the molar mass of elastic chains, no such peaks appear even after keeping the network stretched for over a month, which discounts kinetic effects.

Figure 4 shows spectra characteristic of samples 2-4 in the mesophase. The spectra remain unchanged until the entire sample has been necked, after which increasing the local extension ratio increases the amorphous phase splitting, but the mesophase splitting remains the same. The amorphous component peaks show asymmetric broadening about their maxima. Because the mesophase and amorphous peaks are clearly separated, the spectral areas can be used to calculate the mesophase fraction in the neck region. The fractional area under the mesophase is found to grow with the extension ratio and is around 0.6 for the maximum stretch ratio for samples 2 and 4. This is identical to the maximum extent of mesophase formation observed earlier in PDES networks[6] with deuterated elastic chains. These guest chains therefore remain homogeneously distributed in the networks and act as perfect probes or replicas of their environment.

The top two line shapes in Figure 3 show the spectra of sample 5 in the mesophase. For sample 5, the amorphous phase peak further increases in full width at half-maximum and a doublet with a spitting at 19.1 k Hz appears. Due to the dominance of the methyl $-CD_3$ peak, the mesophase content with increasing extension ratio for sample 5 could not be analyzed quantitatively. The existence of a single 19.1 kHz mesophase splitting corresponding to the methylene deuterons has been explained by Litvinov, Macho, and Spiess,[26] who studied melts of PDES and concluded that there is restricted rotation of the ethylene side chains around the Si–C bonds in the mesophase on the time scale of the NMR measurement.

Figure 5 is characteristic of samples with PDES-d_5 guest chains with a molar mass more than 2 times the
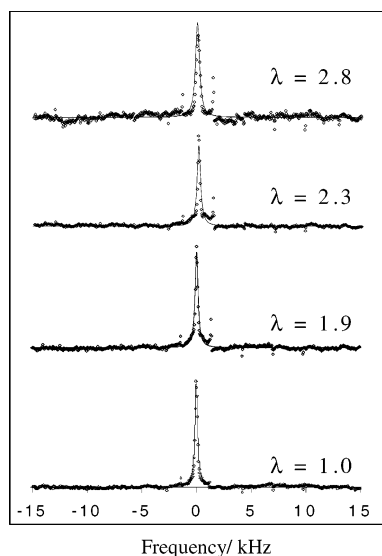
Figure 5. Extension spectra of sample 7. Stretch ratios of 2.3 and 2.8 correspond to the sample in the mesomorphic state.

Figure 6. Corrected "low-q" data for PDES-d_5 fraction I as a function of concentration. The inset is the Zimm representation.

molar mass of network precursor chains (samples 7−11 of Table 2) as they go from the amorphous state to the mesomorphic state. No peak splitting of 19.1 kHz is observed, but the full width at half-maximum of the central methyl peak increases from around 300 to 450 Hz. Thus, we have observed experimentally that guest chains with $M_{n,g}/M_{n,h}$ (molar mass of guest chains to molar mass of host) less than 1.6 were retained in the mesophase, but guest chains with $M_{n,g}/M_{n,h}$ greater than 1.6 were partitioned to the amorphous phase.

Nematic interactions in polymer networks and melts that may include either entropic or energetic interactions or a combination of both have been theoretically modeled by various groups. DiMarzio,[27] Jackson et al.,[28] and Tanaka and Allen[29] developed lattice models with anisotropic interactions that enhanced the alignment of neighboring segments. Jarry and Monnerie[30] included a Maier−Saupe[31] interaction parameter between monomers, along the lines of that introduced by de Gennes[32] to explain interactions in liquid crystals and were able to explain the local ordering in natural rubber. But all these theories considered homogeneous systems and concluded that nematic interactions principally increase the orientation, but mechanical behavior[30] or rheological properties[33,34] are not altered significantly. Very few studies have looked at a two-component system of the kind considered in our study.

A model developed more recently by Olmsted and Milner[35] for strain-induced nematic phase separation in polymer blends and gels, is relevant to the PDES system investigated here because the phase separation described in this model depends on an underlying isotropic−nematic transition. Our PDES chains have a strong nematic interaction (responsible for mesophase formation) and at high strain (local extension ratio greater than 2.2) the networks undergo a phase transition. Olmsted and Milner use a mean-field model that includes a Maier−Saupe interaction between the monomers (i.e., a sole energetic interaction, but the results should be equally applicable for a combination of entropic and energetic interactions). The applied strain is modeled as an external nematic field that applies directly to the host network with the guest chains coupling to the strain indirectly via the host. The condition for thermodynamic stability is derived using
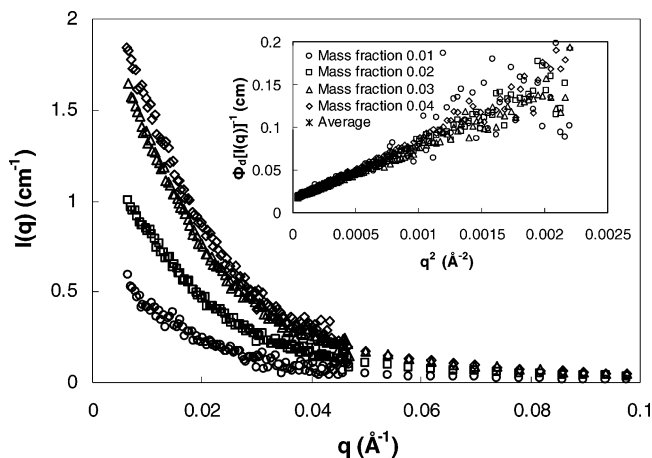
the fact that the host monomers gain free energy when they orient in response to the strain, but not as much as they would in the absence of the guest chains. There is, however, a loss of mixing entropy when the guest chains are segregated from the host. Thus when the gain in nematic free energy exactly compensates the free energy cost of separating the guest from hosts, phase separation occurs. The condition for thermodynamic stability is written as

$$\frac{1}{N_g\phi} - \frac{(\lambda^2 - \lambda^{-1})^2}{N_h^2} \frac{\chi_o^2 w}{1 - \chi_o w} > 0 \qquad (3)$$

where N_h is the number of segments of a host chain, N_g is the number of segments of a guest chain, λ is the stretch ratio, w governs the strength of the nematic interaction, and χ_o is the bare susceptibility through which the host and guest monomers respond to local nematic fields.

From the above inequality four conditions promote phase separation: longer guest chains, more guest chains, stronger nematic interaction, and an increased effective strain. With a comparable volume fraction of guest chains in various networks, the inequality then implies that phase separation will occur for longer chains, as we observe with our samples. Olmsted and Milner indicate that in a one-phase system a decrease in the order parameter of the guest chains relative to the host is a signature of an underlying phase separation. In our two-phase system selective partitioning into the amorphous phase is directly evident by the absence of NMR mesophase peaks.

3.3. SANS Data. 3.3.1. Melts. Figures 6−8 show corrected low q data at different concentrations for fractions I−III, respectively. These data were corrected for incoherent scattering by subtracting PDES-H scattering multiplied by an empirically determined constant from the high-q data. Corrected low-q data were plotted as $\phi_d/I(q)$ vs q^2 (the Zimm representation)[36,37] to calculate the z-average radius of gyration R_{g-z} and weight-average molecular mass M_w.

$$\phi_d/I(q) = (\rho_d/k_n M_w)(1 - q^2 R_{g-z}^2/3 + ...) \qquad (4)$$

where ρ_d is the density of the deuterated species (1.021 g cm^{-3}) and k$_n$ is a scattering contrast factor, equal to 6.174×10^{-4} for this system. The Zimm plots for
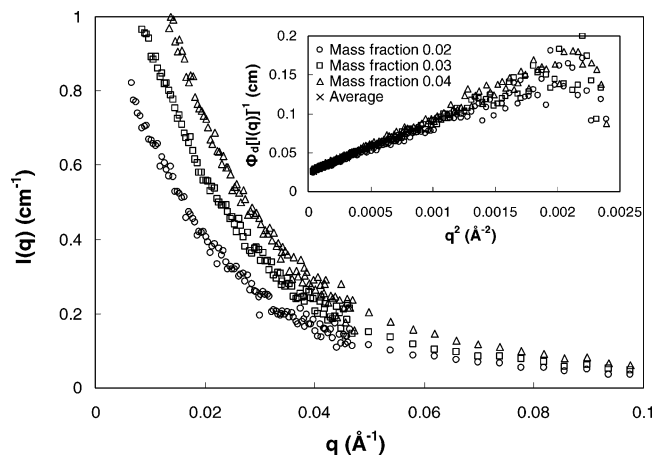
Figure 7. Corrected "low-q" data for PDES-d_5 fraction II as a function of concentration. The inset is the Zimm representation.
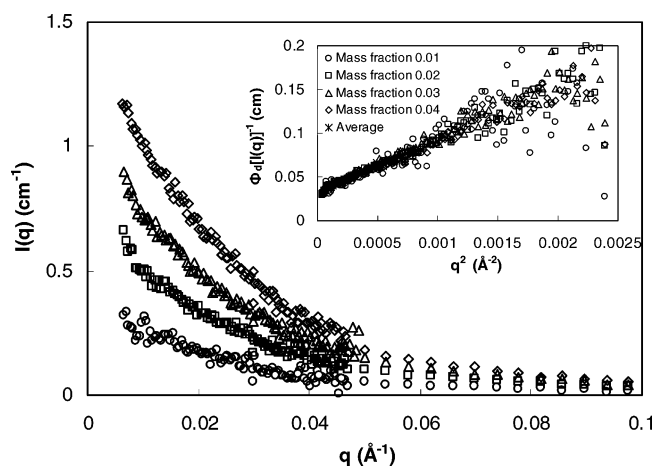

Figure 8. Corrected "low-q" data for PDES-d_5 fraction III as a function of concentration. The inset is the Zimm representation.

fractions I–III shown as insets in Figures 6–8, respectively, are essentially independent of concentration for all fractions studied. The concentration independence of the scattering indicates that the second virial coefficient of PDES-d_5 in the blends is essentially zero. Subsequent analysis of the Zimm plots was therefore conducted by averaging the data over all concentrations rather than extrapolating results to zero concentration. From the averaged data and according to eq 4, weight-average molecular masses for fractions I–III were found to be 99, 65, and 49 kg mol^{-1}, respectively. The corresponding radii of gyration were 107, 89, and 74 Å. Values of M_w calculated from Zimm plots matched GPC polystyrene equivalent molar masses almost identically, lending credence to our SANS data reduction procedure.

3.3.2. Unstretched Networks. Because it was determined that the second virial coefficient of PDES-d_5 in PDES-H is essentially zero, we could extract the radius of gyration of the guest chains in the network from the scattering intensity of a single network sample containing that chain, provided the volume fraction of the guest chains in the network was known accurately. The low-q and high-q data were matched in their overlapping range by multiplying the low-q data by an empirically determined constant. The high-q data were used to calculate the incoherent scattering. The low-q data were then corrected by subtracting this incoherent scattering. Figure 9 shows the corrected low-q data for
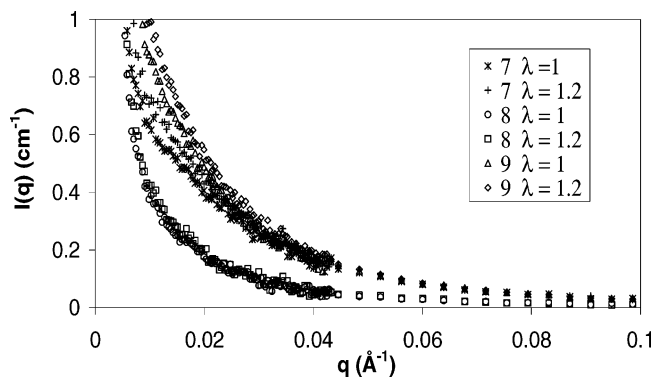

Figure 9. Corrected low-q data for unstretched samples 7–9 and for samples 7–9 at an extension ratio of 1.2.
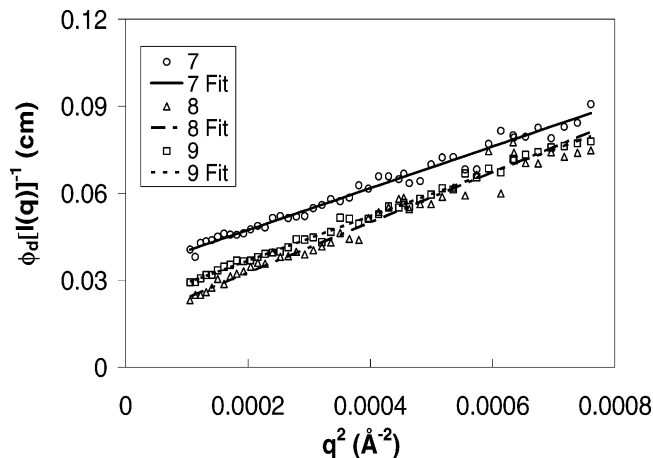

Figure 10. Zimm analysis of samples 7–9 in the unstretched state.

Table 3. Comparison of the Radius of Gyration and Molecular Weight of the Guest Chains in the Melt with Those Dissolved in Networks[a]

fraction	radius of gyration (Å)		wt av mol mass (kg/mol)	
	melt	network	melt	network
d_5–I	107 ± 1	130 ± 3	99 ± 1.0	108 ± 3
d_5–II	89 ± 0.6	103 ± 1	65 ± 0.5	77 ± 1
d_5–III	74 ± 1	80 ± 1	49 ± 0.6	50 ± 0.8

[a] See text for explanation of uncertainties.

samples 7–9 under unstretched and stretched ($\lambda = 1.2$) conditions. To determine the radius of gyration of the probe chains in the unstretched networks, corrected low-q data were plotted in the Zimm representation (Figure 10) to calculate the z-average radius of gyration R_{g-z} and weight-average molar mass M_w. Table 3 compares the values of the radius of gyration of the three fractions of PDES-d_5 in the melt to that in unstretched networks. We note from Table 3 that values of R_{g-z} in the networks are 8–20% larger than the values in the melt. This difference could be attributed to the error in matching the low-q and high-q data in the overlap range and hence an error in the incoherent scattering. These numbers compare well with the only other SANS study on PDES melts.[38]

3.3.3. Stretched Networks. Samples 1 and 7–9 were stretched to a local extension ratio of 1.2 to investigate the effect of stretching on the radius of gyration of the linear guest chains. To accurately measure the thickness of the stretched samples, we used the fact that the incoherent scattering is proportional to the mass of sample illuminated by the beam, and
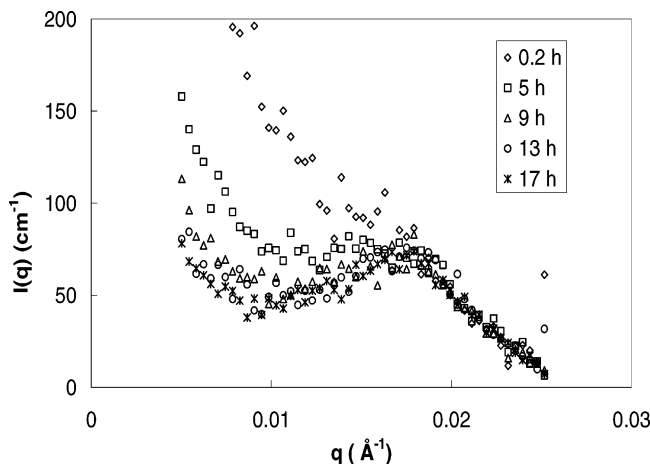
Figure 11. Evolution of scattering intensity for sample 8 as a function of time from stretching the sample in the mesomorphic state.

therefore proportional to the sample thickness. Hence, the high-q data for the stretched sample and the unstretched samples should match. The thickness of the stretched sample was determined by matching the high-q data. As can be seen from Figure 9, the curves from the stretched samples overlap with the curves from the unstretched samples for all q within experimental error. Thus, there is little change in the radius of gyration of the guest chains in networks stretched to λ = 1.2. Similar results were previously reported for guest PDMS chains in compressed PDMS networks.[13] Thus, although ^{2}H NMR is able to easily detect orientation anisotropy at the segment level, there appears to be hardly any discernible effect of the network deformation on the length scale of the radius of gyration of the guest chains.

3.3.4. Networks in the Mesomorphic State. Samples 1 and 7−9 were stretched to a local extension ratio of 2 and held at 0 °C for 2 h to accelerate the formation of the mesophase. The samples were warmed to 5 °C to retain the necked mesomorphic state, and data acquisition was begun immediately. The isointensity plots of the scattering pattern evolved in time. Figure 11 shows the evolution of scattering intensity $I(q)$ for sample 8 obtained by a sector average perpendicular to the direction of stretch with a differential angle of 10° as function of q. At first, there is strong scattering with a large upturn at low q and no peak. That indicates a strongly phase-separated morphology with random structure and concentration fluctuations on many length scales. As time progresses, the upturn at low q weakens and a peak appears at high q, indicating a highly ordered structure has formed. The scattering contrast results from preferential segregation of the deuterated guest chains into the amorphous microdomains. The observation of a peak or upturn in the coherent scattered intensity indicates an enrichment of the deuterated chains in one of the two phases but does not necessarily indicate that either phase is totally devoid of guest chains.

Figure 11 shows that the formation of the mesophase at 5 °C takes approximately 10 h to come to equilibrium. This is the same kinetic time scale for small stretching rate observed by SAXS.[39] Samples 3, 5, 10, and 11 were therefore initially stretched to a local extension ratio of greater than 2.3 and allowed to equilibrate overnight before data acquisition. For each sample three different
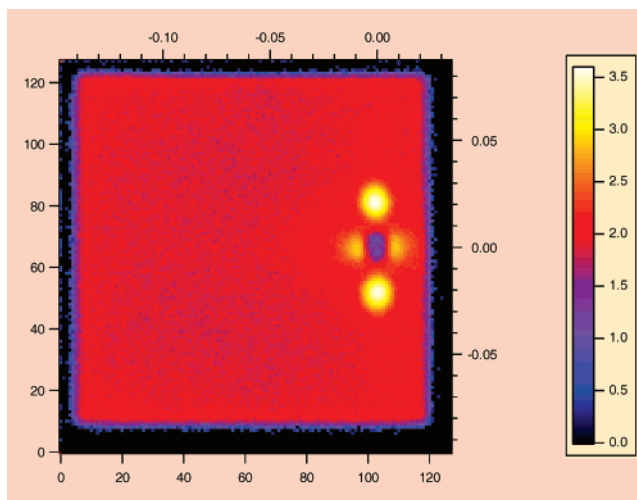

Figure 12. Isointensity plot of the scattering pattern of sample 3 after 12 h of stretching to a local extension ratio of 2.84 in the mesomorphic state.
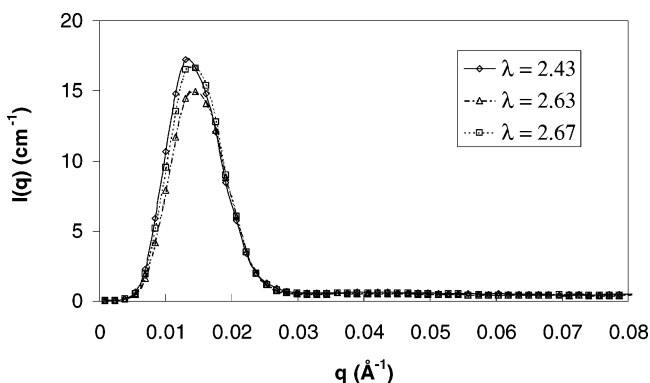

Figure 13. Scattering intensity parallel to the direction of stretch using a rectangular average of pixel width equal to 2 for sample 10 at different local extension ratios in the mesomorphic state.

local extension ratios were investigated. After stretching to a different extension ratio, at least 8−10 h were allowed for the sample to equilibrate.

The isointensity plot of sample 3 in the mesophase at a local extension ratio of 2.84 in Figure 12 shows well-defined spots in the direction parallel to stretch in contrast to smeared out intensities shown in Figure 11 and obtained during development of the mesophase. The well-defined spots in Figure 12 are due to the alignment and ordering of the lamellae in the mesophase. The spot location gives the average domain spacing, and its sharpness indicates very regular ordering of domains in the stretch direction. Figure 13 shows a peak in the $I(q)$ vs q plots obtained at the three stretch ratios by a rectangular average 2 pixels wide in the direction parallel to stretch. This peak position q^* can be related to domain size (d) by Bragg's equation[37]

$$d = \frac{2\pi}{q^*} \tag{5}$$

Scattering from an ideal two-phase lamellar structure in which lamellae of one phase with a uniform thickness alternate with lamellae of the other phase results in Bragg peaks at a series of q values satisfying $q = 2\pi n/d$. The area under the nth-order peak is proportional to $\sin^2(\pi n\varphi_a)/n^2$, where φ_a is the volume fraction of phase A. But, scattering from structures with variable
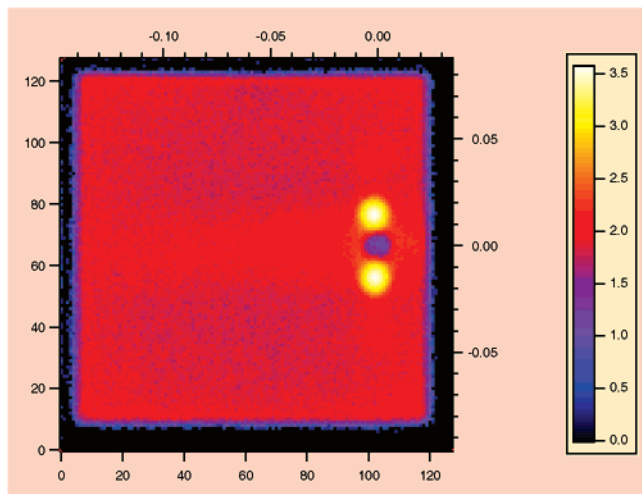
Figure 14. Isointensity plot of the scattering pattern of sample 5 after 12 h of stretching to a local extension ratio of 2.37 in the mesomorphic state.

Table 4. Comparison of Approximate Domain Spacings of the Mesophase As Measured by SANS and SAXS as a Function of Molar Mass of the Network[a]

	SANS		SAXS[39]	
sample	M_n (kg/mol)	domain spacing (Å)	M_n (kg/mol)	domain spacing (Å)
3	21	270	19.9	270
11	23	360	25.7	295
5	27	390	34.4	380

[a] Uncertainties quoted in text.

lamella thickness result in broader peaks and the area under the *n*th-order peak scales as n^{-4}.[37] If the volumes of the two phases are equal, all even-order peaks disappear. This seems to be the case in Figure 13, which is representative of the $I(q)$ vs q plot for samples 3, 5, 10, and 11 and where a very weak third-order peak can be detected. The first peak in Figure 13 ($q \sim 0.014$ Å^{-1}) is broad and the area under the extremely weak third peak ($q \sim 0.04$ Å^{-1}) seems to scale as $^1/_{81}$st rather than $^1/_9$th of the first peak, indicating a variable thickness of the lamellae in these PDES samples.[37]

Figure 14 shows the isointensity plot for sample 5 at a local extension ratio of 2.37 in the mesomorphic state. This figure is also typical of isointensity plots from samples 5, 10, and 11. Perpendicular to the stretch direction there is a spatial variation of the scattering length density (SLD, neutron contrast). However, there is no ordering of the domains in that direction, explaining the lack of well-defined diffraction spots. Rather, the variation of the SLD in this direction is random, resulting in a low-q upturn in the scattering rather than a peak, a common result for randomly structured two-phase materials. As can be seen by comparing Figures 12 and 14 in the direction perpendicular to stretch, the scattering in the direction perpendicular to stretch is more pronounced for sample 3 because it contained a much higher percentage of deuterated chains in comparison to samples 5, 10, and 11. Schlottke[38] has studied two melt samples in the mesophase and observed peaks at approximately $q = 0.15$ Å^{-1} in the scattering intensity plots.

Table 4 shows the variation of domain spacings with molar mass of the precursor chains of the network as measured by SANS. Domain spacings are approximate and were calculated from the q value at which the peak

Table 5. Approximate Spacing of the Mesophase Domains As Measured by SANS as a Function of the Local Extension Ratios in the Fully Necked State[a]

sample	M_n (kg/mol)	λ	domain spacing (Å)
3	21	2.84	270
		2.93	270
		2.98	280
11	23	2.83	360
		2.96	390
5	27	2.37	380
		2.60	390

[a] Uncertainties quoted in text.

SANS intensity was observed. Domain spacings are comparable to those obtained by SAXS in a previous study.[39] For the three samples considered, the effective molecular weight between cross-links is similar because the networks have the approximately the same modulus G_e/RT (approximately 60 mol m^{-3}), so the variation of domain size correlates exclusively with the molar mass of the precursor chains. As pointed out earlier, the volume fraction of the crystalline phase in the mesomorphic state is approximately 50%, as inferred from SANS intensity plots and, therefore, the thickness of the crystalline lamellae is approximately half the domain spacing reported in Table 4. For sample 11 the thickness of the crystalline lamellae is thus 18 nm. The length of a completely extended PDES chain of molar mass M_n can be estimated from the equation[40] $L = (c/2)(M_n/M_0)$, where $c = 0.475$ nm is the length along the chain axis of a unit cell containing two monomer units and $M_0 = 102.2$ is the molar mass of the monomer unit. For sample 11 that has a precursor molar mass of 23k, the length of a fully extended PDES chain is thus calculated to be 53.5 nm. The fully extended chain length is thus approximately 3 times the thickness of a crystalline domain, and longer precursor chains would allow for the formation of larger domains, as has been previously observed in SAXS studies.[39] Near the cross-link points, the chains cannot form a mesophase due to the starlike structure around cross-link. The variation of domain spacing with local extension ratio is weak for samples 3, 5, and 11, as shown in Table 5, and this is also consistent with earlier SAXS results that cover a wider range of extension ratios.

4. Conclusions

We exploit the ability of PDES networks to form a strain-induced mesophase to demonstrate the tendency of larger guest chains to partition selectively to the amorphous phase and the tendency of the smaller guest chains to remain homogeneously distributed through the mesophase and the amorphous phase. ^{2}H NMR spectra provide unambiguous evidence of phase separation (via the absence of mesophase peaks). Phase separation is thought to occur when the gain in free energy due to the extra orientation of the host in the absence of the guest chains equals the free energy cost of segregation. The unique nature of PDES elastomers allows observation of phase separation of guest chains that would have been difficult to observe directly otherwise.[35] We also show that for the guest chains in the amorphous region of stretched PDES networks, the segment orientation is similar to that of the elastic chains, which can be explained in terms of a combination of excluded volume and energetic interactions. The radius of gyration of the probe chains in the stretched

(20% extension) and unstretched state were found from SANS to be identical to that in the melt state. The scattering intensity from a SANS pattern for a network with guest chains of any size has a strong first-order peak and a much weaker third-order peak in the direction parallel to stretch. The peak positions were used to calculate the domain spacing of the lamellae in the mesophase as well as the average lamellae thickness that was found to be approximately one-third of the fully extended elastic chain length. These submicrometer domain spacings compare well with results from SAXS and scale with the precursor molecular weight of the elastic chains. The domain sizes are almost independent of the local extension ratio in the fully necked samples.

References and Notes

(1) Warner, M.; Wang, X. J. *Macromolecules* **1991**, *24*, 4932.
(2) Out, G. J. J.; Turetskii, A. A.; Snijder, M.; Möller, M.; Papkov, V. S. *Polymer* **1995**, *36*, 3213.
(3) Godovsky, Y. K. *Angew. Mackromol. Chem.* **1992**, *202/203*, 187.
(4) Hedden, R. C. Ph.D. Dissertation, Cornell University, 2000.
(5) Wunderlich, B.; Grebowicz, J. *Adv. Polym. Sci.* **1984**, *60/61*, 1.
(6) Hedden, R. C.; Tachibana, H.; Duncan, T. M.; Cohen, C. *Macromolecules* **2001**, *34*, 5540.
(7) Hedden, R. C.; McCaskey, E.; Cohen, C.; Duncan, T. M. *Macromolecules* **2001**, *34*, 3285.
(8) Cohen-Addad, J. P.; Dupeyre, R. *Polymer* **1983**, *24*, 400.
(9) McLoughlin, K.; Waldbieser, J. K.; Cohen, C.; Duncan, T. M. *Macromolecules* **1997**, *30*, 1044.
(10) Brereton, M. G.; Ries, M. E. *Macromolecules* **1996**, *29*, 2644.
(11) Boué, F.; Farnoux, B.; Bastide, J.; Lapp, A.; Herz, J.; Picot, C. *Europhys. Lett.* **1986**, *12*, 637.
(12) Liu, X.; Bauer, B.; Briber, R. *Macromolecules* **1997**, *30*, 4704.
(13) Gilra, N.; Cohen, C.; Briber, R. M.; Bauer, B. J.; Hedden, R. C.; Panagiotopoulos, A. Z. *Macromolecules* **2001**, *34*, 7773.
(14) Gilra, N.; Panagiotopoulos, A.; Cohen, C. *Macromolecules* **2001**, *34*, 6090.
(15) Hedden, R. C.; Saxena, H.; Cohen, C. *Macromolecules* **2000**, *33*, 8676.
(16) Hedden, R. C.; Cohen, C. *Polymer* **2000**, *41*, 6975.
(17) Gent, A. N.; Tobias, R. H. *J. Polym. Sci., Polym. Phys. Ed.* **1982**, *20*, 2317.
(18) de Gennes, P.-G. *Scaling Concepts in Polymer Physics*; Cornell University Press: Ithaca, NY, 1979.
(19) Hammouda, B.; Krueger, S.; Glinka, C. J. *J. Res. Natl. Inst. Stand. Technol.* **1993**, *98*, 31−46.
(20) Prask, H. J.; Rowe, J. M.; Rush, J. J.; Schroeder, I. G. *J. Res. Natl. Inst. Stand. Technol.* **1993**, *98*, 1−13.
(21) Flory, P. J. *Principles of Polymer Chemistry*; Cornell University Press: Ithaca, NY, 1953.
(22) Kuhn, W.; Grun, F. *Kolloid Z.* **1942**, *101*, 248.
(23) Deloche, B.; Beltzung, M.; Herz, J. *J. Phys. Lett.* **1982**, *43*, 763.
(24) Sotta, P.; Deloche, B.; Herz, J.; Lapp, A.; Durand, D.; Rabadeux, J. C. *Macromolecules* **1987**, *20*, 2769.
(25) Jacobi, M.; Abetz, V.; Stadler, R.; Gronski, W. *Polymer* **1996**, *37*, 1669.
(26) Litvinov, M.; Macho, V.; Spiess, H. W. *Acta Polym.* **1997**, *48*, 471.
(27) DiMarzio, E. A. *J. Chem Phys.* **1962**, *36*, 1568.
(28) Jackson, J. L., Shen, M. C.; McQuarrie, D. A. *J. Chem. Phys.* **1966**, *44*, 2388.
(29) Tanaka, T.; Allen, G. *Macromolecules* **1977**, *10*, 426.
(30) Jarry, J.-P.; Monnerie, L. *Macromolecules* **1979**, *12*, 316.
(31) Maier, W. and Saupe, A. *Z. Naturforsch. A* **1959**, *14*, 882.
(32) de Gennes, P. G. *The Physics of Liquid Crystals*; Clarendon: Oxford, U.K., 1975.
(33) Doi, M.; Pearson, D.; Kornfield, J.; Fuller, G. *Macromolecules* **1989**, *22*, 1488.
(34) Merill, W. W.; Tirrell, M.; Tassin, J.-F.; Monnerie, L. *Macromolecules* **1989**, *22*, 896.
(35) Olmsted, P. D.; Milner, S. T. *Macromolecules* **1994**, *27*, 6648.
(36) Ylitalo, C. M.; Zawada, J. A.; Fuller, G. G.; Abetz, V.; Stadler, R. *Polymer* **1992**, *33*, 2949.
(37) Roe, R.-J., *Methods of X-ray and Neutron Scattering in Polymer Science*; Oxford University Press: Oxford, U.K., 2000.
(38) Schlottke, H. Ph.D. Dissertation, University of Mainz 1995.
(39) Koerner, H.; Luo, Y.; Li, X.; Cohen, C.; Hedden, R. C.; Ober, C. K. *Macromolecules* **2003**, *36*, 1975.
(40) Godovsky, Y. K.; Papkov, V. S.; Magonov, S. N. *Macromolecules* **2001**, *34*, 976.
(41) Certain commercial materials and equipment are identified in this paper to adequately specify the experimental procedure. In no case does such identification imply recommendation by the National Institute of Standards and Technology nor does it imply that the material or equipment is the best available for this purpose.